AD-A044 399 HONEYWELL INC BLOOMINGTON MINN CORPORATE MATERIAL SC--ETC F/G 9/1
CRACK PROPAGATION IN PZT.(U)
JUL 77 J G BRUCE, B G KOEPKE N00014-76-C-0625

UNCLASSIFIED NL

| OF |
AD
A044399

END
DATE
FILMED
10-77
DDC

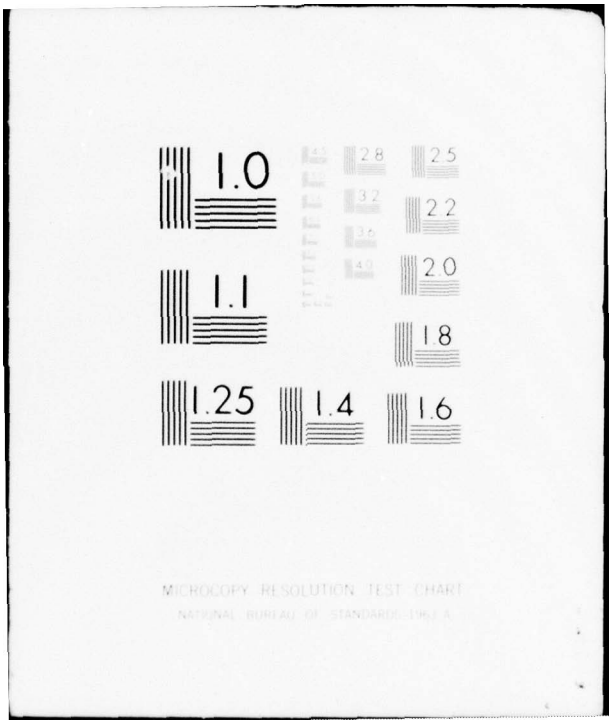
1.0
1.1
1.25
1.4
1.6
2.8
2.5
3.2
2.2
3.6
2.0
4.0
1.8
MICROCOPY RESOLUTION TEST CHART
NATIONAL BUREAU OF STANDARDS-1963-A

CRACK PROPAGATION IN PZT

First Technical Report

by

J. G. Bruce and B. G. Koepke
Honeywell Corporate Material Sciences Center

Office of Naval Research Project CG103
Contract No. N00014-76-C-0625/P00002

July 1977

Honeywell Inc.
Corporate Material Sciences Center
10701 Lyndale Avenue South
Bloomington, Minnesota 55420

(12)

(6) CRACK PROPAGATION IN PZT.

(9) First Technical Report,

by

(10) J. G. Bruce and B. G. Koepke
Honeywell Corporate Material Sciences Center

(15) Office of Naval Research Project CG103
Contract No. N00014-76-C-0625/P00002

(11) July 1977

(12) 45p.

Honeywell Inc.
Corporate Material Sciences Center
10701 Lyndale Avenue South
Bloomington, Minnesota 55420

ABSTRACT

Subcritical crack propagation in the transducer ceramic, PZT, has been studied using the double torsion technique. The effects of testing environment and temperature, as well as the state of poling in the material, have been characterized in detail. Tests run in water and in environments inert with respect to water such as toluene, mineral oil and Freon, a corona suppressant, have established that water enhances slow crack propagation in PZT. Fracture has also been found to depend sensitively on the state of poling. Crack propagation is hindered if poling is perpendicular to the crack plane but is hardly affected if the material is poled parallel to the crack. These results can be explained more in terms of the residual stresses introduced by poling than in terms of the microstructural (i.e., domain structure) changes accompanying poling. A thermal activation analysis carried out on crack propagation data measured in water on unpoled PZT yielded a stress free activation energy of 100 kcal/mol.

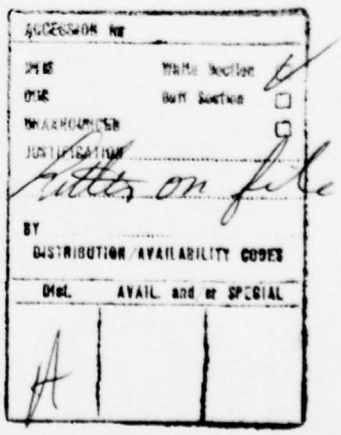

TABLE OF CONTENTS

LIST OF ILLUSTRATIONS

LIST OF ILLUSTRATIONS (Concluded)

I. INTRODUCTION

The propagation of surface and subsurface flaws under subcritical* loads in a ceramic high-drive sonar transducer can be detrimental to both the mechanical strength and the electrical characteristics of the device. The mechanical properties degrade since the fracture stress, σ_F, of a brittle material depends sensitively on the initial flaw size, a, through the Griffith equation $\sigma_F = AK_{IC}a^{-1/2}$ where A is a geometrical term on the order of unity and K_{IC} is the critical stress intensity factor (i.e., the fracture toughness). The electrical characteristics can be altered by flaw growth since flaws are sites of corona discharge. Electrical discharge contributes to noise to the device. If the device output is increased or if the unit is subjected to shock loading, both these concerns are amplified.

The piezoelectric properties of sonar transducer ceramics such as barium titanate and solid solutions of lead zirconate and lead titanate (PZT) have been intensively studied and improved through the addition of a host of elements (many proprietary)[1]. The mechanical properites, particularly the fracture characteristics, on the other hand, have only recently attracted attention[2, 3].

Recent work at the Naval Research Laboratory has identified predominant fracture origins in PZT as pores, pore clusters, large grains, and machining flaws[3, 4]. Origins of surface fracture have also been observed at the edges of electrodes on transducer elements in regions of high electric field gradients[5]. Pohanka, et. al. [6] have further shown that internal

---

*A subcritical load is any load less than that necessary to catastrophically propagate the flaw.

stresses resulting from the paraelectric → ferroelectric phase transformation occurring in PZT upon cooling through the Curie temperature can measurably decrease the fracture resistance of the material.

The phenomenon of subcritical crack growth has been studied in many ceramic materials[7] but has only recently been investigated in transducer ceramics. Freiman et. al.[8] published data showing that water enhances slow crack growth in PZT5800 (a Navy Type I material), and Caldwell and Bradt[9] established that slow crack growth in PZT could be detected using dynamic fatigue tests* in both three-point bend and in compressive tests.

These studies have established that subcritical crack growth occurs in PZT and the effect is sensitive to the chemical environment. More work is needed, however, to determine in greater detail the effects of chemical environment on flaw growth in a transducer ceramic, particularly with respect to the effects of temperature and to the effects of realistic transducer operating environments such as corona suppressants. In addition, it is not known how the microstructural changes introduced by poling affect crack growth. In $BaTiO_3$, Freiman et. al[8] observed an enhancement of crack propagation in samples poled parallel to the crack plane. The effects of poling perpendicular to the crack plane have not been reported.

In this report we present the results of an extensive series of measurements in which slow crack growth in PZT was examined in a number of testing environments. The effects of temperature on crack propagation in one environment (water) are reported for the first time. Finally, the anisotropic effects of poling on slow crack growth are demonstrated by testing specimens poled both parallel and perpendicular to the crack plane.

*In dynamic fatigue tests, σ_F is measured as a function of stressing rate. If subcritical crack growth occurs during loading, σ_F is expected to increase with loading rate since less flaw growth takes place during the shorter tests.

II. EXPERIMENTAL PROCEDURE

A. LOAD RELAXATION TESTING

Slow crack growth in PZT was studied using the double torsion (DT) technique popularized by Evans et. al.[10, 11]. A schematic showing the specimen and loading geometry is shown in Figure 1. The stress intensity for this configuration is independent of crack length and is given by

$$K_I = PW_m\left[\frac{3(1+\nu)}{Wd^3d_n}\right]^{1/2} = AP \qquad (1)$$

where P is the load, ν is Poisson's ratio, and the other terms are defined on the Figure. Slow crack growth was studied using the load relaxation technique. In a load relaxation test a precracked specimen is rapidly loaded to a load, P, somewhat less than the critical load, P_{IC}, necessary to initiate fast fracture of the specimen; and the crosshead of the testing machine is arrested. If slow crack growth occurs, the load will decay as a function of time since the compliance of the system is an increasing function of crack length. Providing the compliance is a linear function of crack length, it can be shown that the crack velocity is related to the instantaneous load and the rate of decay of the load according to[11]

$$V = \frac{-(P_{i,f})(a_{i,f})}{P^2}\left(\frac{dP}{dt}\right) \qquad (2)$$

where $P_{i,f}$ and $a_{i,f}$ are initial (or final) load and crack length respectively. Thus, in a single load relaxation test, V is measured over a range of K_I. The results are usually plotted as log V vs. log K_I since log V is experimentally found to be a linear function of log K_I for many ceramics[7, 12].

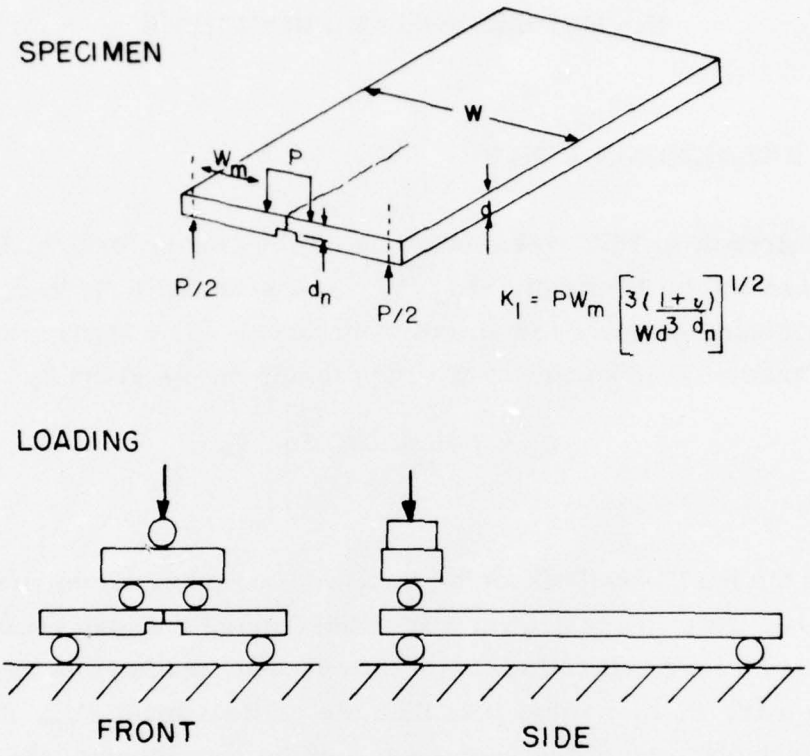

Figure 1. Schematic showing specimen and loading geometry for double torsion tests.

The samples used in the tests were PZT plates nominally 2.54 cm (1 in.) wide, 7.62 cm (3 in.) long and had thicknesses ranging from 15 mm (0.060 in.) to 23 mm (0.090 in.). A side groove was cut in each specimen to a depth of about one-half the specimen thickness and to a width of approximately 3 mm. We will comment on the side groove width in more detail in the results. The loading jig was copied from one used at the National Bureau of Standards [13] in which the specimen is loaded through four ball bearing as shown in Figure 1. The specimen is supported on the base of the jig by four ball bearings. Before testing, a thin starter notch was cut in the end of the specimen to a depth of 3 mm, and a short scratch was diamond scribed on the bottom of the specimen at the base of the notch to ensure that a crack would initiate down the center of the side groove.

In a typical test a specimen was tested with the side groove up. (i.e. opposite to that shown in Figure 1). This facilitated the determination of the final crack length with dye penetrant at the termination of a load relaxation test. The specimen was loaded in an Instron TM testing machine at a crosshead speed of 5×10^{-3} mm/min (2×10^{-4} in./min) until a crack popped in as noted by a rapid decrease in the load. The specimen was then unloaded and reloaded at a crosshead speed of 0.25 mm/min (10^{-2} in./min) until the crack just started running, at which time the crosshead was arrested. The load vs. time curve during relaxation was recorded on teletype tape to facilitate computer analysis of the data. The duration of most tests was 15 to 20 minutes since under ordinary testing conditions slight oscillations in the load due to small thermally induced deformations in the loading train will obscure the data at the extremely low relaxation rates occurring at longer times (e.g., those corresponding to $V < 10^{-6}$ m/s).[10]

In computing the $V\text{-}K_I$ curves, provisions were made in the program to include machine relaxations during the test. Accordingly, a background relaxation tape was recorded at a load of approximately one-half to three-fourths P_{IC} before a test. This relaxation was then subtracted from the total relaxation. After the test the final crack length was measured with a dye penetrant.* K_{IC} was then measured by reloading the specimen to failure at a crosshead speed of 0.25 mm/min (10^{-2} in./min).

B. MATERIAL AND TESTING ENVIRONMENT

The PZT specimens tested in this study were cut from transducer tubes manufactured by the Honeywell Ceramics Center. The PZT is a Navy Type III high drive sonar ceramic with a nominal composition of $Pb_{0.94}Sr_{0.06}Ti_{0.47}Zr_{0.53}O_3$ plus proprietary additions. This composition is tetragonal

*Turco Products Inc. "Dy-chek".

below the Curie point and is dielectrically "hard". The tubes were manufactured by cold isostatic pressing and sintering. All samples were cut from unpoled tubes with a 100-grit diamond cut-off wheel and subsequently surface ground to shape with a 100-grit diamond wheel. All grinding was carried out wet.

Samples were tested in liquid environments by immersing the DT loading jig in the fluid in a covered stainless steel chamber. The liquids used were water, toluene, Freon, and mineral oil. The latter three are considered inert with respect to water. Freon, in addition, is a known corona suppressant. The stainless steel chamber had resistance heating elements attached to it to enable tests to be run at elevated temperatures.

C. POLED SPECIMENS

The effects of poling on crack propagation were studied using the composite DT specimen shown in Figure 2. The specimen was produced by first poling a 5 mm wide PZT beam and then cementing it between two wider unpoled PZT beams with high strength epoxy. A side groove was then machined in the poled section and the surfaces trued before testing. A narrow center section is necessary when testing poled specimens because of the high field needed for poling. To produce a high field, the electrode spacing must be kept small. For poling, the sides of each PZT beam were first coated with silver-filled epoxy electrodes and then attached to copper leads. The samples were immersed in Fluorinert Electronic Liquid FC-70* maintained at 150 ± 5°C and a 35 KV/cm field was applied for 2.5 minutes. After poling, the samples were immediately removed from the bath. The poling field was not applied for longer times due to the danger of microcracking the samples[2]. Composite DT specimens were fabricated from the poled material with the direction of polarization both parallel to and perpendicular to the crack plane as shown in Figure 2.

*3M Corp.

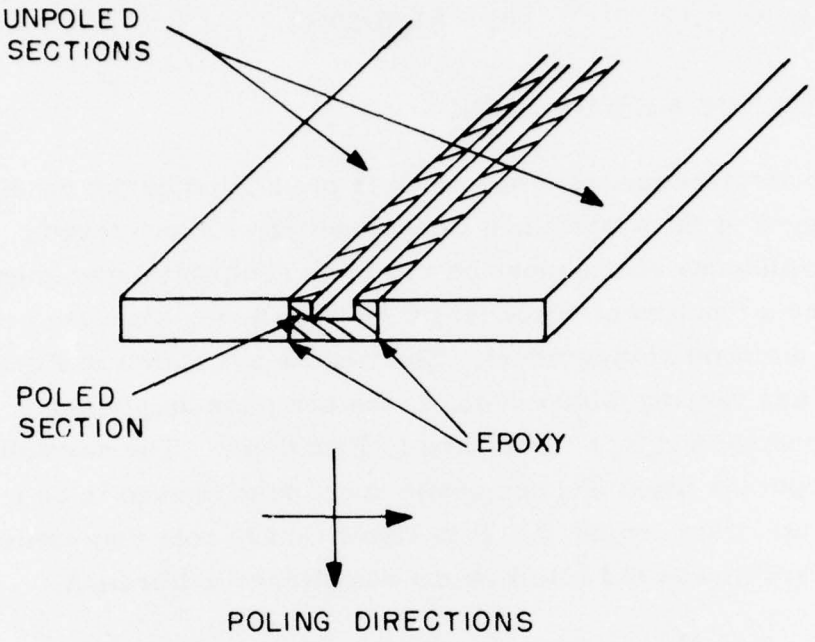

Figure 2. Schematic showing composite PZT double torsion specimen with poled center section cemented between two unpoled sections.

III. RESULTS

A. COMPLIANCE MEASUREMENTS

The elastic analysis for a DT specimen is predicated by the condition that the compliance of the system is a linear function of crack length. To this end the compliances of a number of uncut and composite specimens were measured as a function of crack length by introducing simulated cracks with a thin diamond slicing wheel. The results are shown in Figure 3. Since specimens had varying thicknesses, t, the compliances plotted in Figure 3 have been normalized by t^3 according to Equation 3. The normalized compliance of both the uncut and composite specimens is seen to be a linear function of the crack length, a. It is significant to note that cutting and rejoining the specimens did not alter the compliance calibration.

The theoretical compliance of a DT specimen is given by[11]:

$$C = \frac{Y}{P} \simeq \frac{3W_m{}^2 a}{Wt^3 G} \qquad (3)$$

where Y is the deflection, P is the load, and G is the shear modulus. The other terms are defined in Figure 1. If we let $G = C_{44}{}^E = 2.56 \times 10^4 MNm^{-2}$, i.e., the short circuit value of the shear modulus of Sr modified PZT[1], then $\frac{d(ct^3)}{da} = 8.76 \times 10^{-5} \frac{m^3}{MN}$ $(5.1 \times 10^{-8} \frac{in.^3}{lb.})$. This is nearly identical to the experimental slope of the line shown in the Figure, indicating that the elastic analysis[11] can be applied with confidence in this case to both the uncut and the composite specimens.

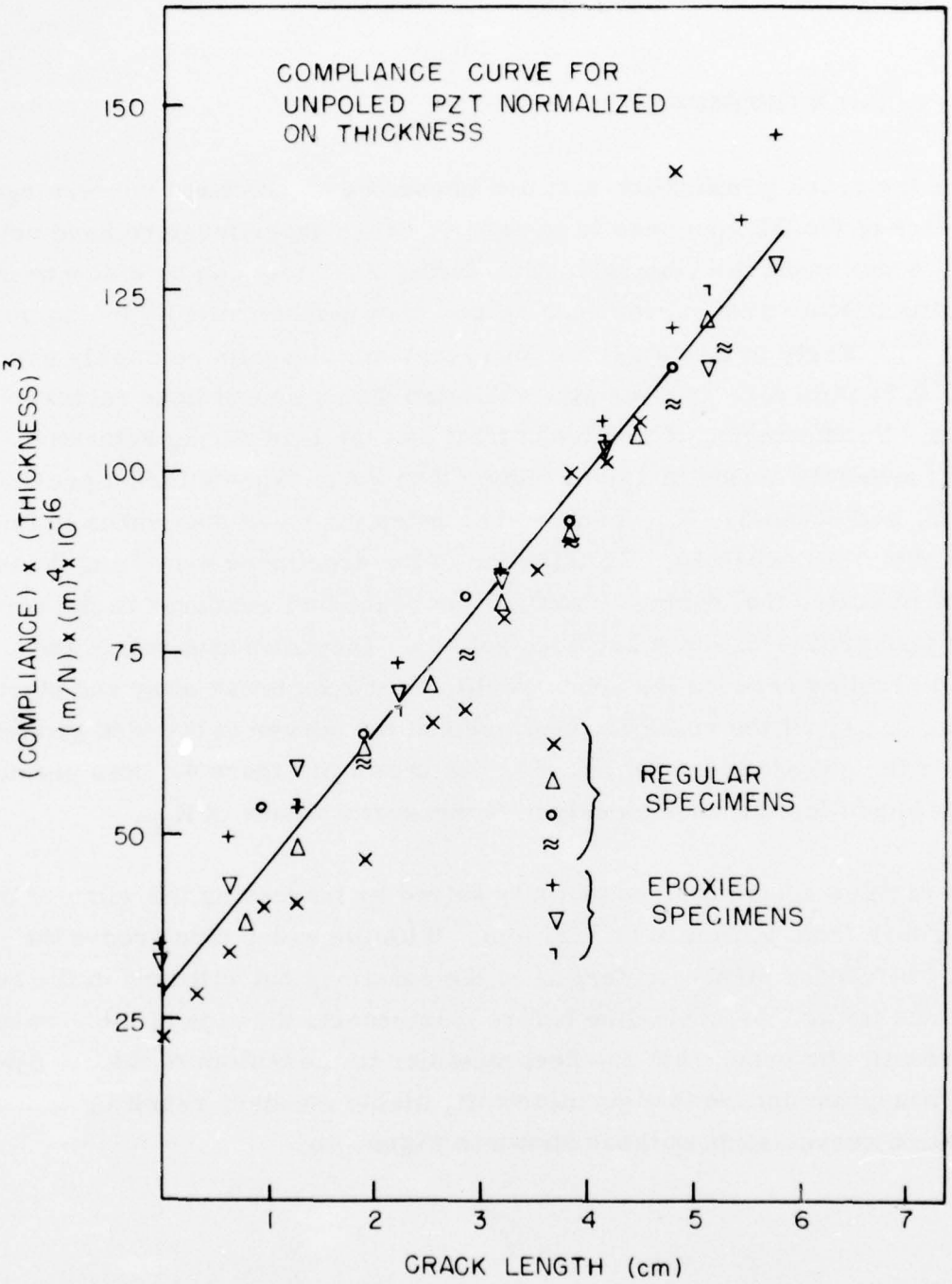

Figure 3. Compliance of regular and composite PZT double torsion specimens plotted as a function of crack length. The compliance has been normalized by t^3 where t is the specimen thickness.

B. SPECIMEN GEOMETRY

Before the crack propagation data are presented, a comment concerning the geometry of the DT specimen is in order. Other experimenters have noted that in some cases the load relaxation during a DT test can be discontinuous, resulting in load-time curves such as that shown schematically in Figure 4a[14, 15]. Early in this study we found that samples with relatively narrow (i.e., 0.75 mm) side grooves also exhibited discontinuous load relaxation curves. Furthermore, it was found first that the load during relaxation would frequently arrest at values higher than those expected from previous results, and secondly, K_{IC} measured by retesting these specimens to failure was higher than expected. Examination of the specimens exhibiting these effects indicated that during relaxation the crack had wandered to the corner of the size groove where it had been held up. Discontinuous relaxation curves resulted because the crack would sometimes break away and start running again. If the crack trapped itself at the corner of the side groove, it would fan out and increase in area. As shown in Figure 4a, this presumably accounts for the anomalously high measured values of K_{IC}.

These problems have been essentially solved by increasing the width of the side groove from 0.75 mm to 3.25 mm. With the wider side groove the crack can wander off the centerline of the specimen but will turn in the stress field back toward the centerline before it intersects the side of the groove. As a result, the crack remains perpendicular to the bottom of the specimen and propagation occurs in a geometrically stable manner, resulting in load relaxation curves such as those shown in Figure 4b.

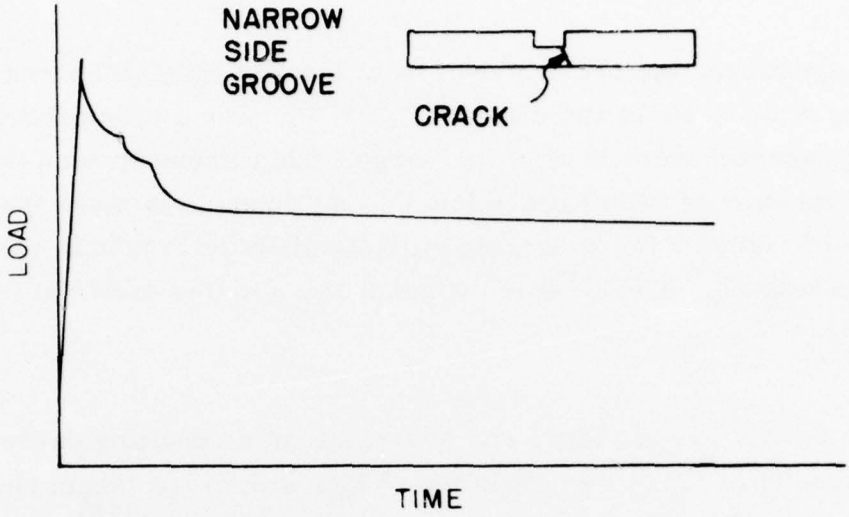

(a) DISCONTINUOUS LOAD RELAXATION CURVE

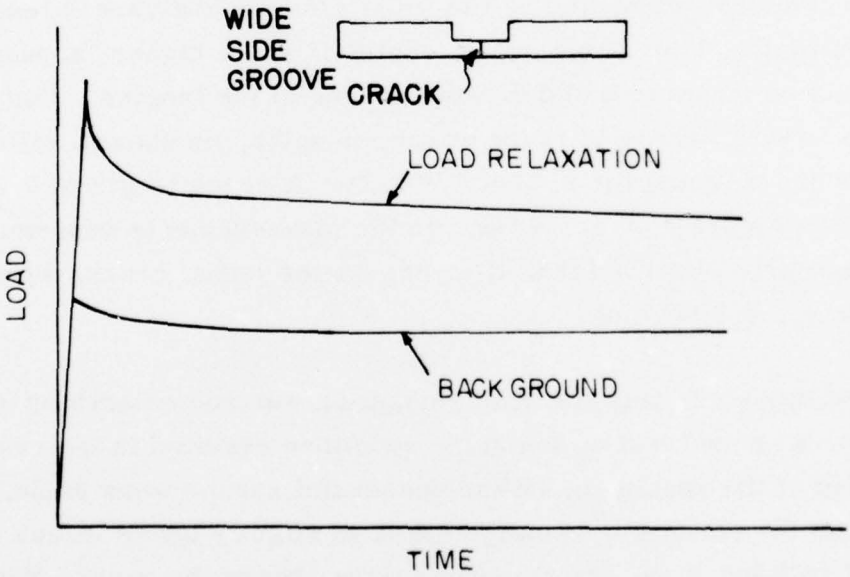

(b) TYPICAL LOAD RELAXATION AND BACKGROUND CURVES

Figure 4. Schematics showing load relaxation curves obtained with narrow and wide side grooves. The background relaxation that is subsequently subtracted from the total relaxation is also illustrated in the bottom sketch.

In a DT specimen, the crack should be at least as long as one-half the specimen width to avoid end effects[11, 15, 16]. For a crack shorter than this, the apparent value of K_I is too large. This is easily seen by measuring K_{IC} as a function of initial crack length. An example of these measurements is shown in Figure 5 for soda-lime-silicate glass microscope slides tested at 25°C in toluene. The accepted value of K_{IC} for this material is 7.5 x $10^5 Nm^{-3/2}$[17]

When the cracks are too long, end effects cause a resulting decrease in the apparent value of K_{IC}. The variation of K_{IC} with crack length shown in Figure 5 is similar to that reported by Shetty and Virkar[18] and to that computed by Trantina[16]. Trantina[16] has performed a three-dimensional elastic finite element stress analysis on the DT specimen and has shown that the value of K_I computed by the finite element analysis is less than that given by Eq. 1 for short crack lengths (i.e., a higher "apparent" value of K_I would be measured) and greater at long crack lengths. For a specimen with L/W=3, where W is the specimen width, he showed valid K_I measurements can be made for $0.54<a/W<2.34$. A crack length of 0.55 W is indicated on Figure 5 by an arrow. In the measurements reported here, it was generally observed that after pop-in-the initial cracks were about 1.3 cm (i.e., 0.5 W) long.

In most of this work only one load relaxation was run on each specimen. Typically, a second test on the same specimen resulted in the crack running out the end of the specimen. When successful reruns were made, the V-K_I curve from the rerun was usually shifted to slightly lower values of K_I. The slopes of both log V vs. log K_I curves were always the same. Whether better absolute values of K_I for V-K_I curves can be obtained using multiple relaxations on the same sample can only be determined on specimens longer than the ones used for this study. It could be pointed out, however, that good reproducibility has been obtained with single relaxations run on a large number of specimens containing different initial crack lengths.

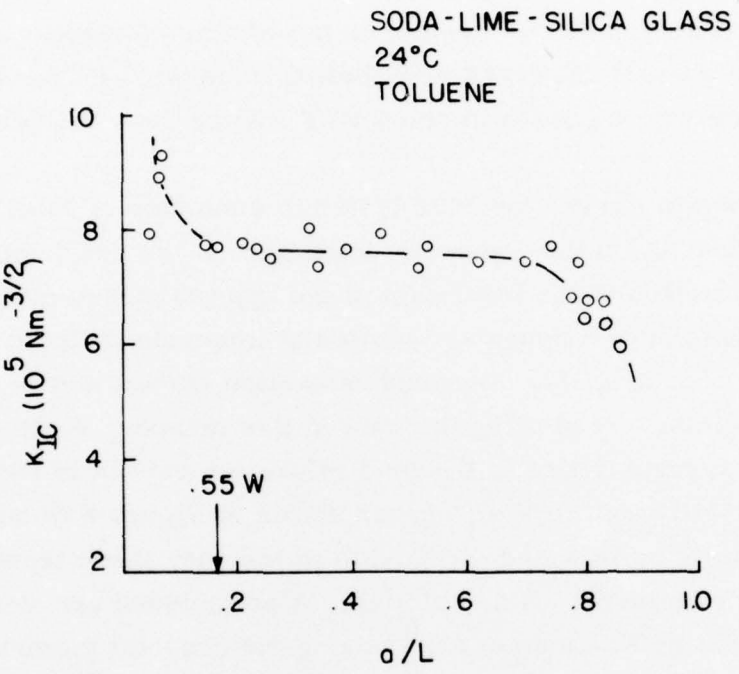

Figure 5. K_{IC} measured in toluene on soda lime silicate glass slides as a function of crack length.

C. ENVIRONMENTAL EFFECTS ON SLOW CRACK GROWTH

In this section we report our results on the effects of various environments on the rate of subcritical crack propagation in unpoled PZT. Environmental effects on slow crack growth in poled PZT will be reported later.

Slow crack growth curves for PZT tested in a number of environments are shown in Figure 6. In the figure the logarithm of the crack velocity, V, is plotted as a function of the logarithm of the applied stress intensity, K_I. The individual points on the figure are plotted at intervals dictated by the computer program used to analyze the load relaxation curves and do not represent actual data points. By plotting the data in this manner, scatter in the data due to minor irregularities in the load relaxation curves is readily visualized. The reproducibility of the $V-K_I$ curves shown in Figure 6 is quite good. Data from five tests in water, five tests in toluene, three tests in Freon, and two tests in mineral oil are plotted. Also included are $V-K_I$ data for PZT 5800 taken by Freiman et al.[8] using the constant moment technique[19]. The fracture toughness, K_{IC}, of this material is low with respect to that of other oxide ceramics such as alumina[7, 10] and is about the same as that for soda-lime-silicate glass (i.e., $0.75 MNm^{-3/2}$).

The data can be conveniently discussed in terms of the three-stage $V-K_I$ curves exhibited by many materials and shown schematically in Figure 7[7, 10]. Water is shown to measurably enhance subcritical propagation in PZT as it does in other crystalline ceramics and glasses[7, 8, 10, 12, 19, 20]. The data for water are in Stage I of the $V-K_I$ curve and can be represented by $V=AK_I^n$. The line drawn on Figure 6 through the water data shows n is on the order of 55. The water data agree reasonably well with that of Freiman et al.[8]. Water-free environments such as toluene, Freon, and mineral oil act to retard slow crack growth. The toluene data exhibit all three stages of the

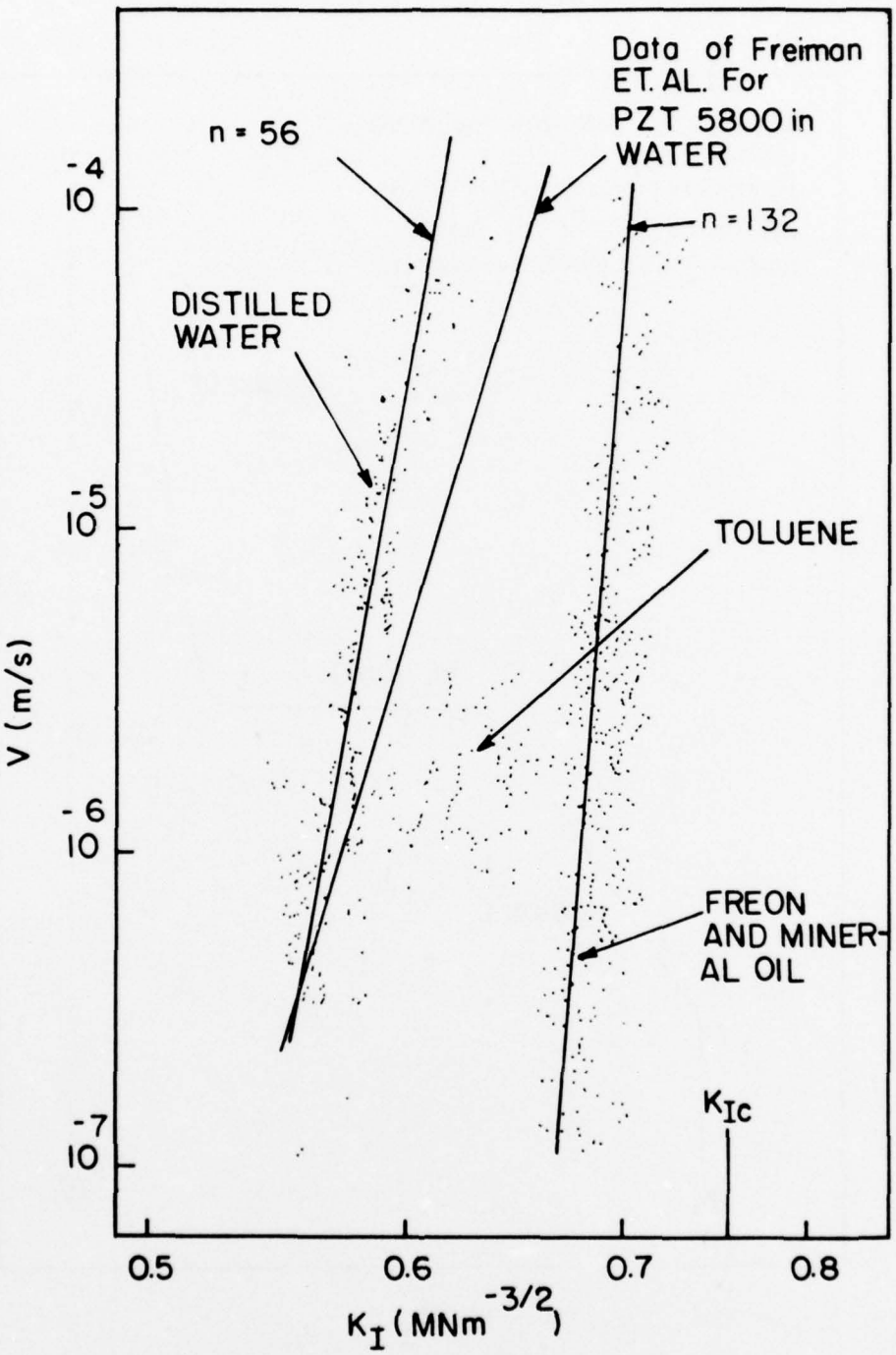

Figure 6. Crack velocity in unpoled PZT measured as a function of applied stress intensity in a number of environments at room temperature. The fracture toughness, K_{IC}, is also indicated on the figure.

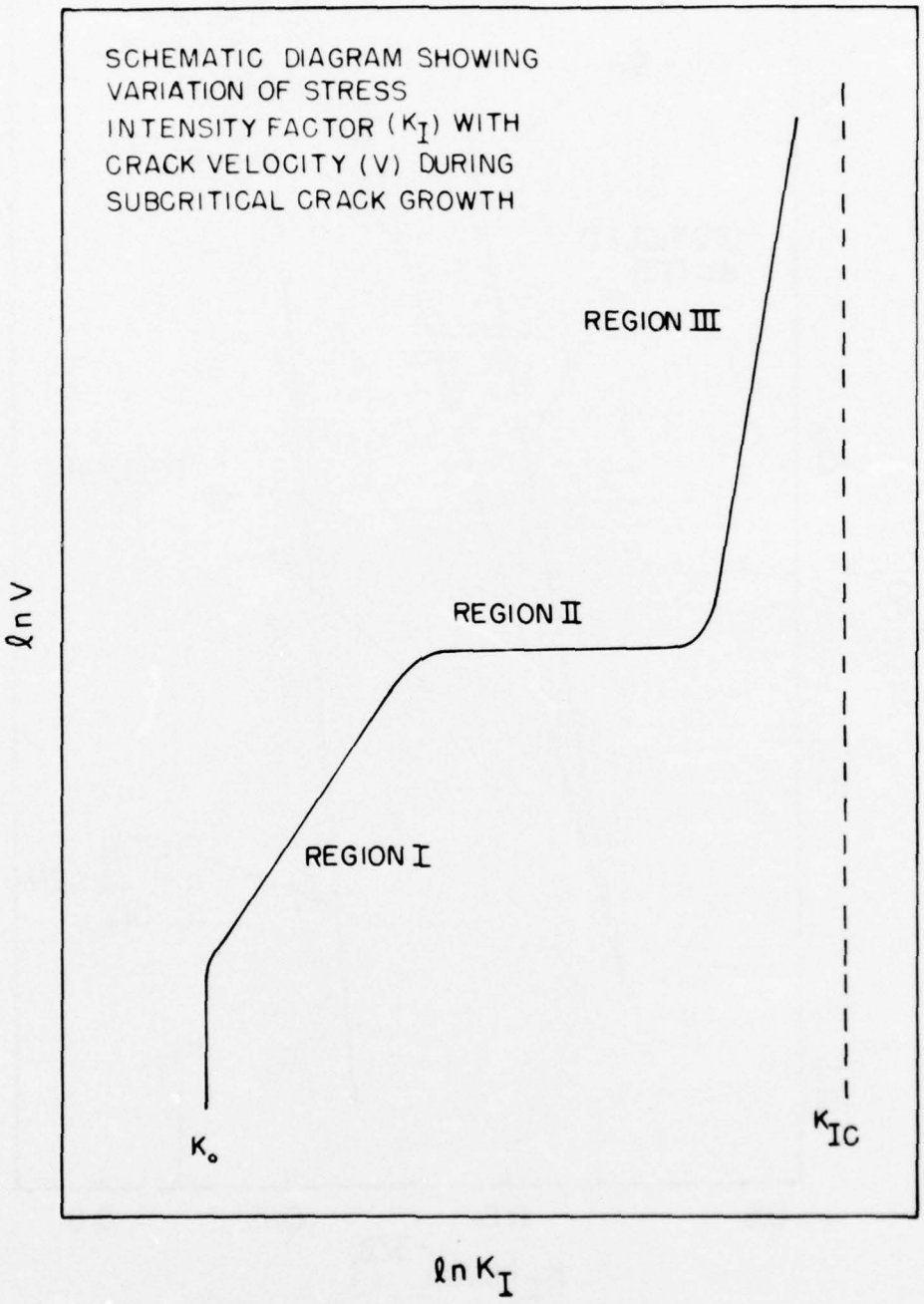

Figure 7. Schematic showing different stages of V-K_I curves exhibited by a large number of materials.

$V\text{-}K_I$ curve while only Stage III crack propagation is observed in the velocity range examined when tests were run in Freon and mineral oil. The slope of the $V\text{-}K_I$ curve in Stage III is about 130. It is noteworthy to point out again that Freon is a recognized corona suppressant.

Slow crack growth in PZT can also be material dependent. Figure 8 shows data taken on PZT from another batch of the same material. Similar effects of environment were noted but the data is shifted by about 0.5 $MNm^{-3/2}$ to higher values of K_I. Thus, when the sometimes subtle effects of testing environment on slow crack growth are examined, it is important to use material from the same batch.

The "high K_I" and "low K_I" materials were further examined to determine if other properties showed similar shifts. A large number of measurements were made of the grain size, fracture strength in three-point bending, and Knoop microhardness of samples cut from both materials. The fracture toughness, grain sizes, fracture strengths, and hardnesses are listed below in Table 1.

Table 1. Characterization of "High K_I" and "Low K_I" PZT

Material	K_{IC}*	Average Grain Size**	Fracture Strength***	Microhardness****
High K_I	$0.73 MNm^{-3/2}$	3.4μm	$77.8 \pm 5.2 MNm^{-2}$	304±8 (19 tests)
Low K_I	$0.69 MNm^{-3/2}$	3.7μm	$82.0 \pm 12.7 MNm^{-2}$	284±5 (27 tests)

* in distilled water

** linear intercept method

*** 3-point bend, 2.54 cm span, 0.125 cm/min loading rate

**** 600-gm load applied for 1 minute

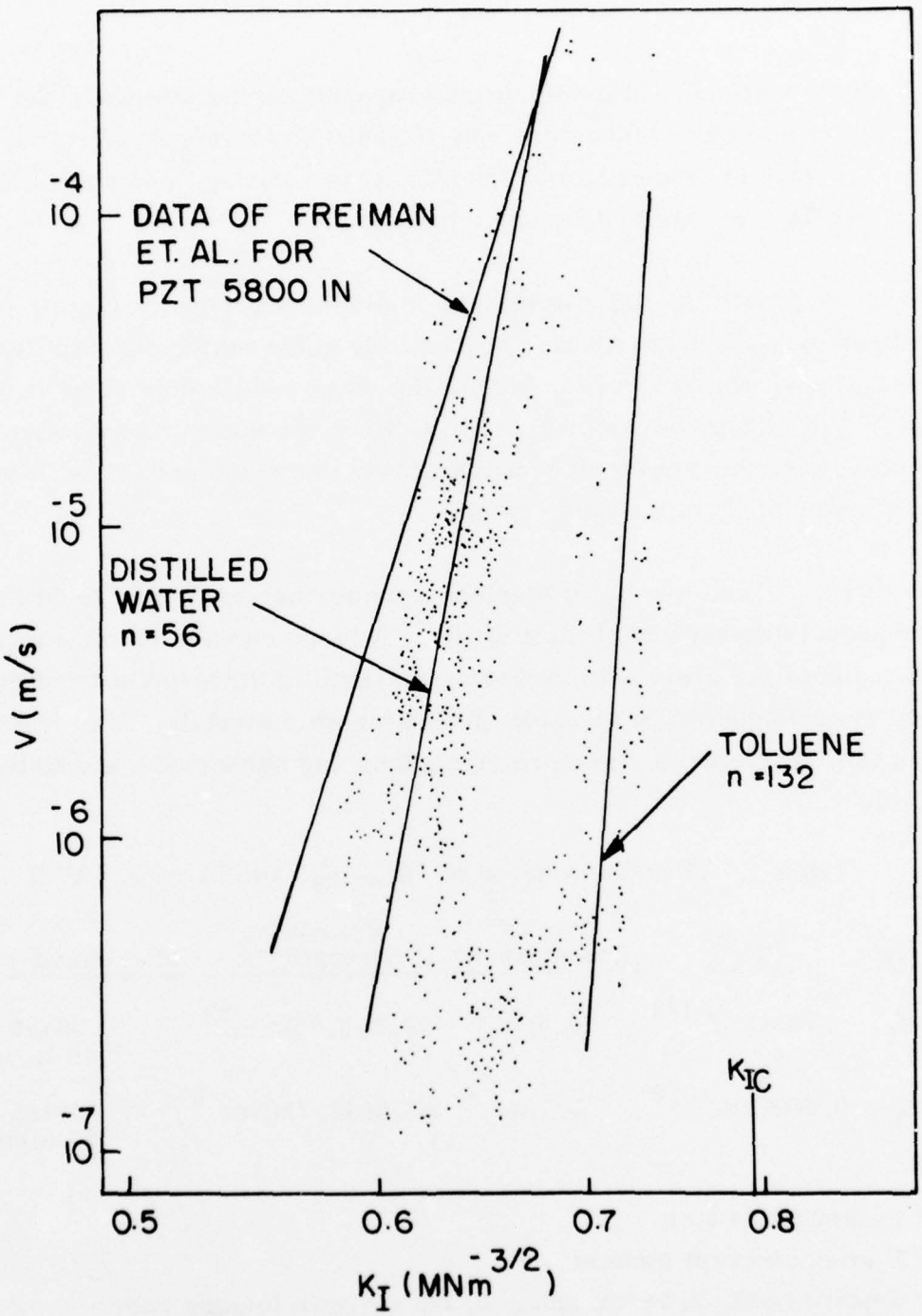

Figure 8. V-K_I data measured in different environments on a different batch of unpoled PZT. Comparison with the "low K_I" data in Figure 6 shows that batch-to-batch variation can be observed in this material.

The grain sizes and fracture strengths of both types of material were essentially the same. The difference in microhardness was significant, however, with the "high K_I" material being harder. If fracture takes place during identation, the hardness number for the "high K_I" material would be expected to be higher. Evans et. al[7, 21] have shown, in fact, that measurements of this type can be used to measure K_{IC}. We did not observe macroscopic cracks at the indentations but cannot discount microcracking. From the above we conclude that the property measurements listed in Table 1 did not aid in revealing the source of the observed differences in fracture resistance of the two batches of material.

D. EFFECTS OF TEMPERATURE ON CRACK PROPAGATION

In order to examine the effects of temperature on slow crack propagation in PZT and to determine if the kinetics of crack growth could be described by some thermally activated process, $V\text{-}K_I$ curves were determined on unpoled samples tested in distilled water at 0°, 25°, 50°, and 75°C and in mineral oil at 25°, 75°, 100°, and 125°C. All the samples for each series of tests were cut from the same transducer tube (from the "low K_I" batch) to reduce sample to sample variation. $V\text{-}K_I$ curves for the samples tested in water are shown in Figure 9. At lease two runs at each temperature are plotted. The data for $V > 10^{-6}$ m/s were fitted to $V = AK_I^n$ with the least squares approach and the values of the exponents are indicated on Figure 9. We note that the crack velocity increases with increasing temperature. If slow crack growth in PZT is thermally activated and if a single process is rate controlling, the crack velocity can be written as

$$V = V_o \exp(-E^* + \alpha K_I)/RT$$

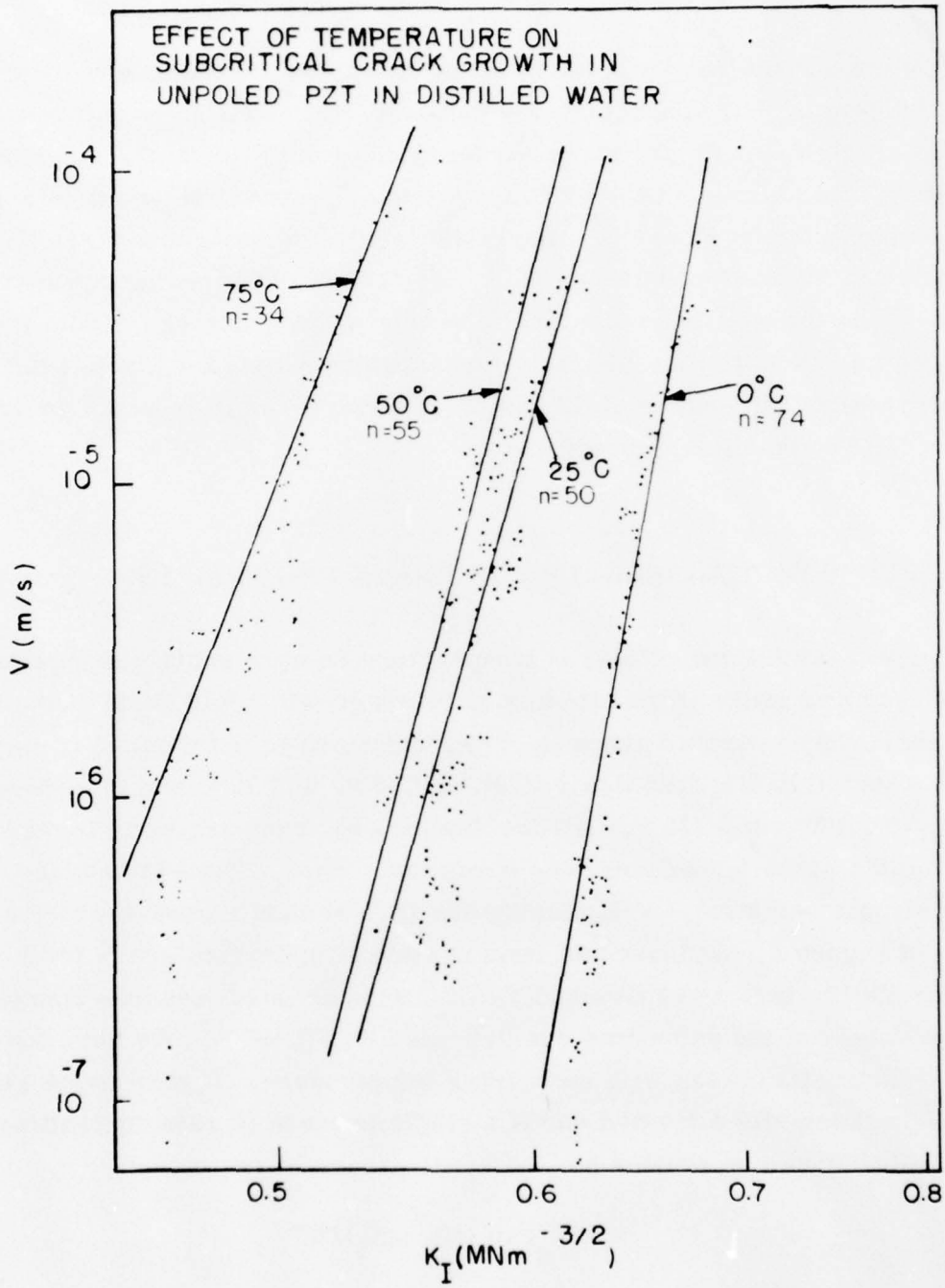

Figure 9. Effect of temperature on crack propagation in unpoled PZT measured in distilled water.

where $E^* - \alpha K_I$ is the apparent activation energy for fracture. E^* is the stress free activation energy and V_o and α are constants[22]. The activation volume is contained in α. In Figure 10 the velocity at constant K_I (from Figure 9) is plotted as a function of temperature. From least squares fits of these data the apparent activation energy can be plotted as a function of the applied stress intensity as shown in Figure 11. E^* is approximately 100 kcal/mole. Similar tests were run in mineral oil but the results were ambiguous. Figure 12 shows $V-K_I$ curves for PZT in mineral oil at temperatures ranging from 25° to 100°C. Note first that n decreases rapidly from 25° to 75°C and then remains about constant to 100°C. $V-K_I$ curves measured at 125°C were identical to those at 100°C. This behavior is not indicative of a single thermally activated mechanism and cannot be treated as such. Either the chemical nature of the oil is changing or the mechanical properties (and fracture mechanism) are changing discontinuously with temperature.

E. EFFECTS OF POLING ON CRACK PROPAGATION IN PZT

In this section we discuss crack propagation obtained on poled material. In view of the batch to batch differences in fracture behavior noted earlier, all the poled specimens were prepared from "low K_I" material. The poled samples exhibited a remanent polarization of about 25×10^{-6} coul/cm^2.* The maximum remanent polarization in this material is about 38×10^{-6}coul/cm^2.

The effects of testing environment on slow crack growth of PZT poled perpendicular to the crack (see Figure 2) are shown in Figure 13. Included on the figure are data taken in distilled water (four tests), toluene (three tests) and mineral oil (two tests). Comparing Figures 6 and 13, we note that the major effect of poling on environmentally sensitive slow crack growth in

*Measured at the Honeywell Ceramics Center

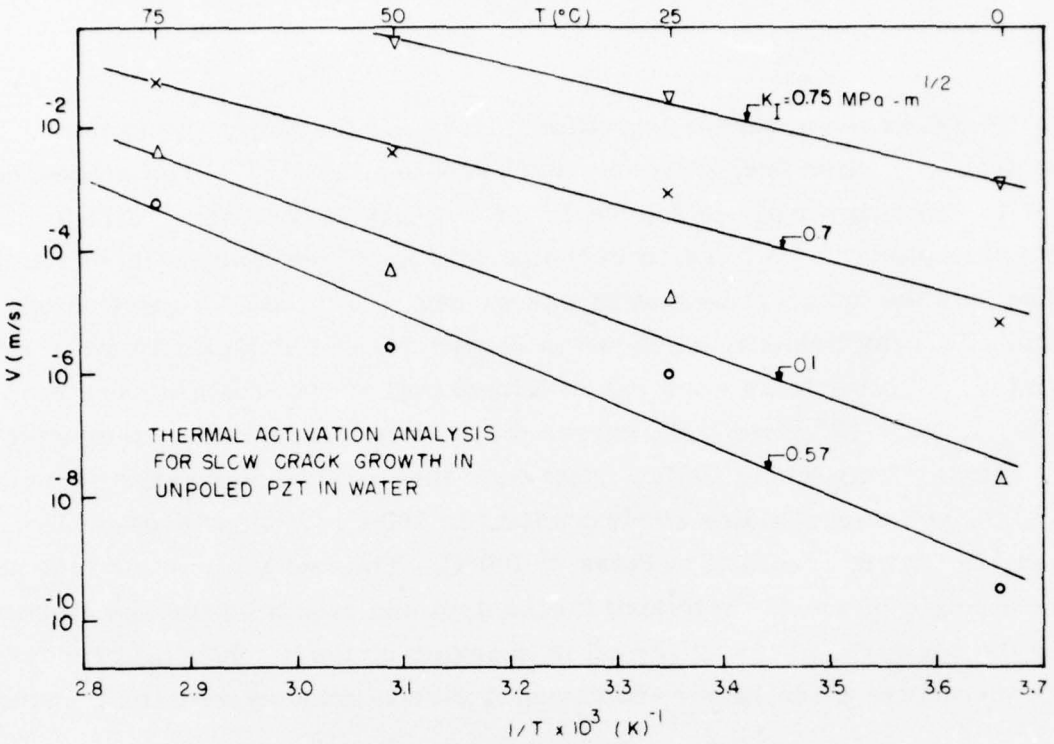

Figure 10. Data of Figure 9 replotted to show crack velocity as a function of temperature at different values of applied stress intensity.

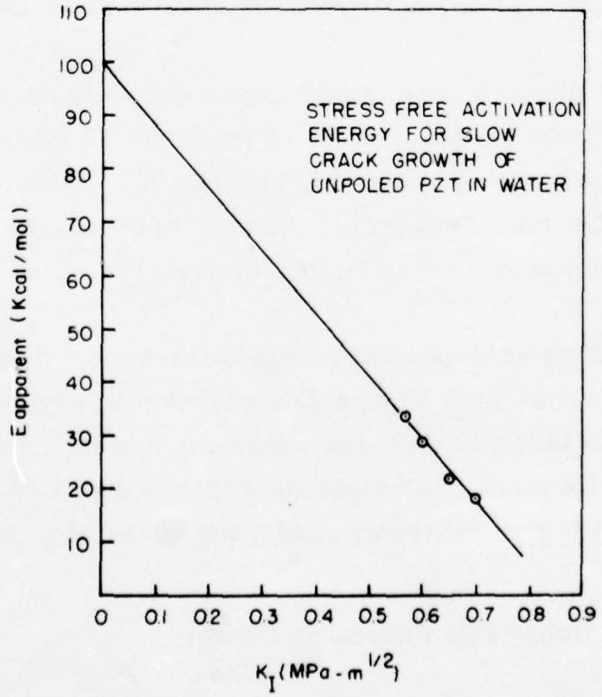

Figure 11. Apparent activation energy for crack propagation in unpoled PZT in water plotted as a function of applies stress intensity.

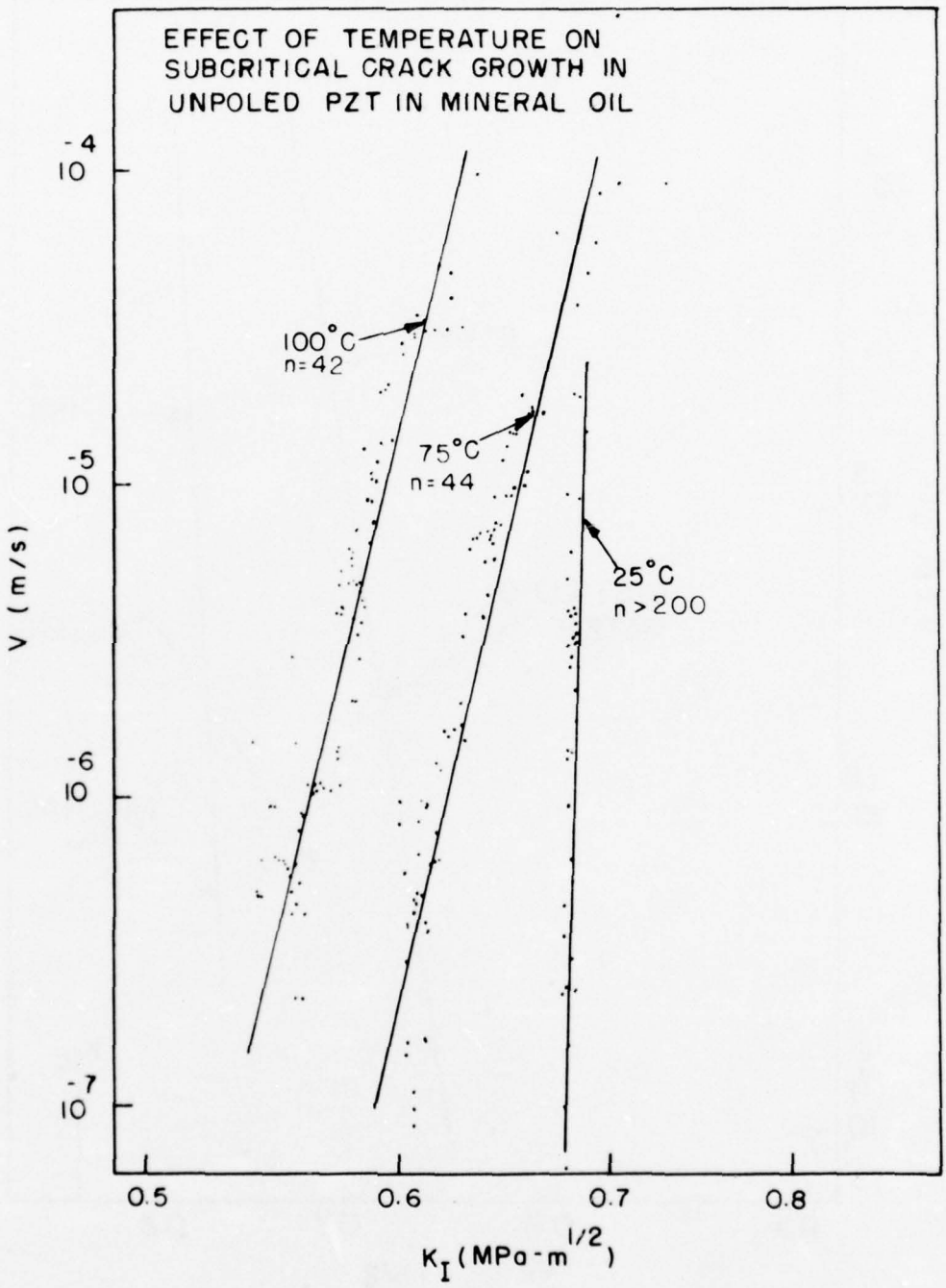

Figure 12. Effect of temperature on crack propagation in unpoled PZT measured in mineral oil.

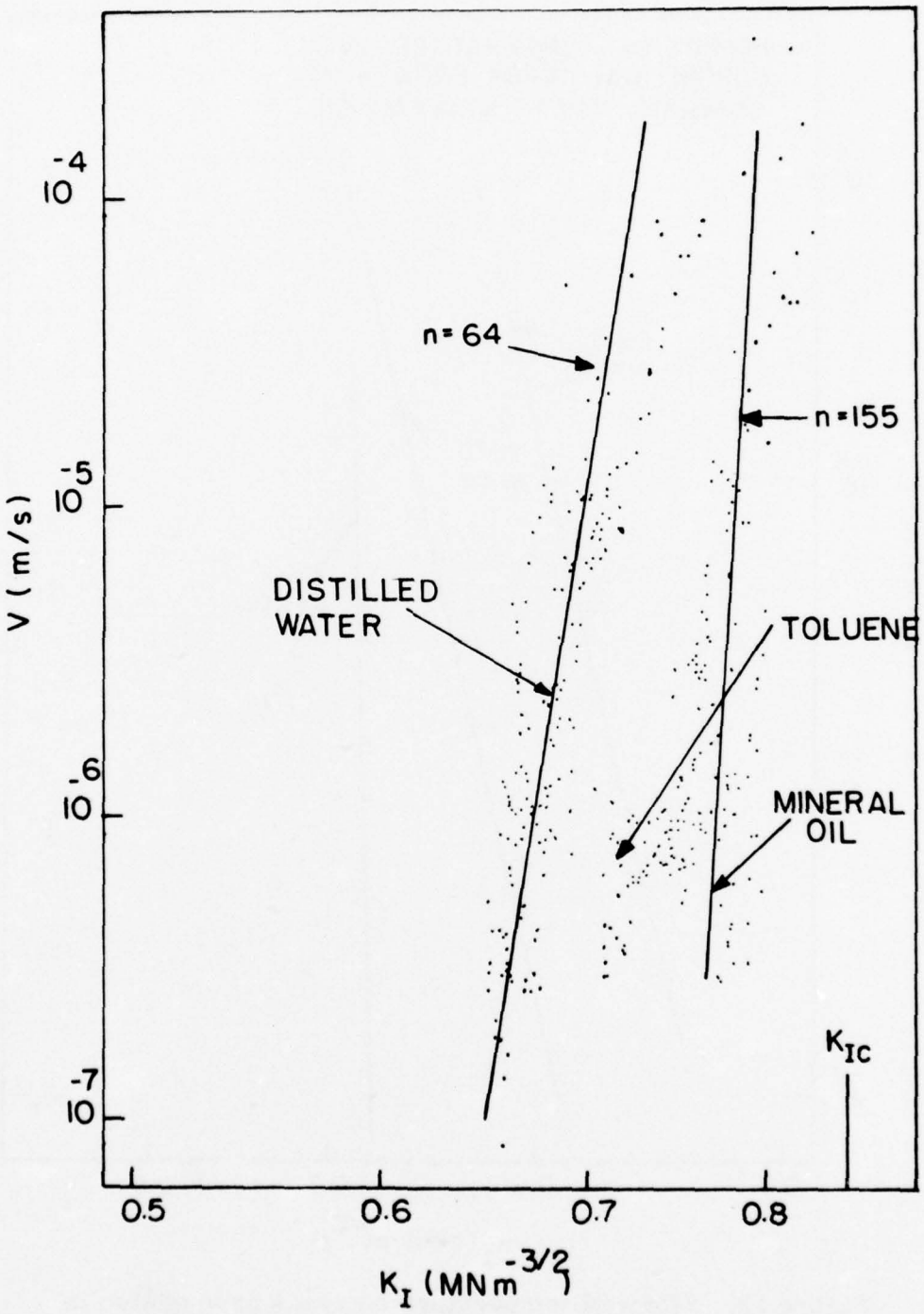

Figure 13. The effect of environment on crack propagation in PZT poled perpendicular to the crack. Poling has shifted the curves to higher values of K_I.

PZT is to displace the V-K_I curves by about 0.1MNm$^{-3/2}$ to higher K_I values. The slopes of the curves in Stage I (i.e., water) and in Stage III (i.e., mineral oil and toluene) are slightly higher in the poled material but the significance of the difference is questionable in view of the scatter in the data. Samples poled parallel to the crack plane were only tested in distilled water. The range of these data along with those for other material tested in water at ambient temperature are shown in Figure 14. Note that poling parallel to the crack had little effect on the V-K_I curves.

F. CRACK PROFILES, FRACTURE SURFACES, AND MICROSTRUCTURES

As a result of the loading geometry in a double torsion test, the crack profiles are curved as shown schematically in Figure 15 [7, 10, 11]. If crack propagation is assumed to be orthogonal to the crack front (this has not been experimentally verified for PZT), the crack velocity given by Equation 2 is too high but can be approximately adjusted by the correction factor $\phi = d_n / (c^2+d_n^2)^{1/2}$ [10, 11]. Photographs of two crack profiles in PZT are also shown in Figures 15b and 15c. The profiles represent the crack shape following a high loading rate test to failure to determine K_{IC}. A dotted line has been drawn on the photos of the top specimen half in Figures 15b and 15c to better reveal the crack profile. Based on these observations and others, $\phi \simeq 0.45$. The data presented in this report have all been corrected by that amount.

Close examination of some of the crack profiles showed they meet the bottom surface at an angle greater than 90 degrees. An example is shown in Figure 15c. This is attributed to the presence of grinding induced compressive stresses in the near surface layers of the specimen. Nadeau (23) has observed similar profiles in vitreous carbon.

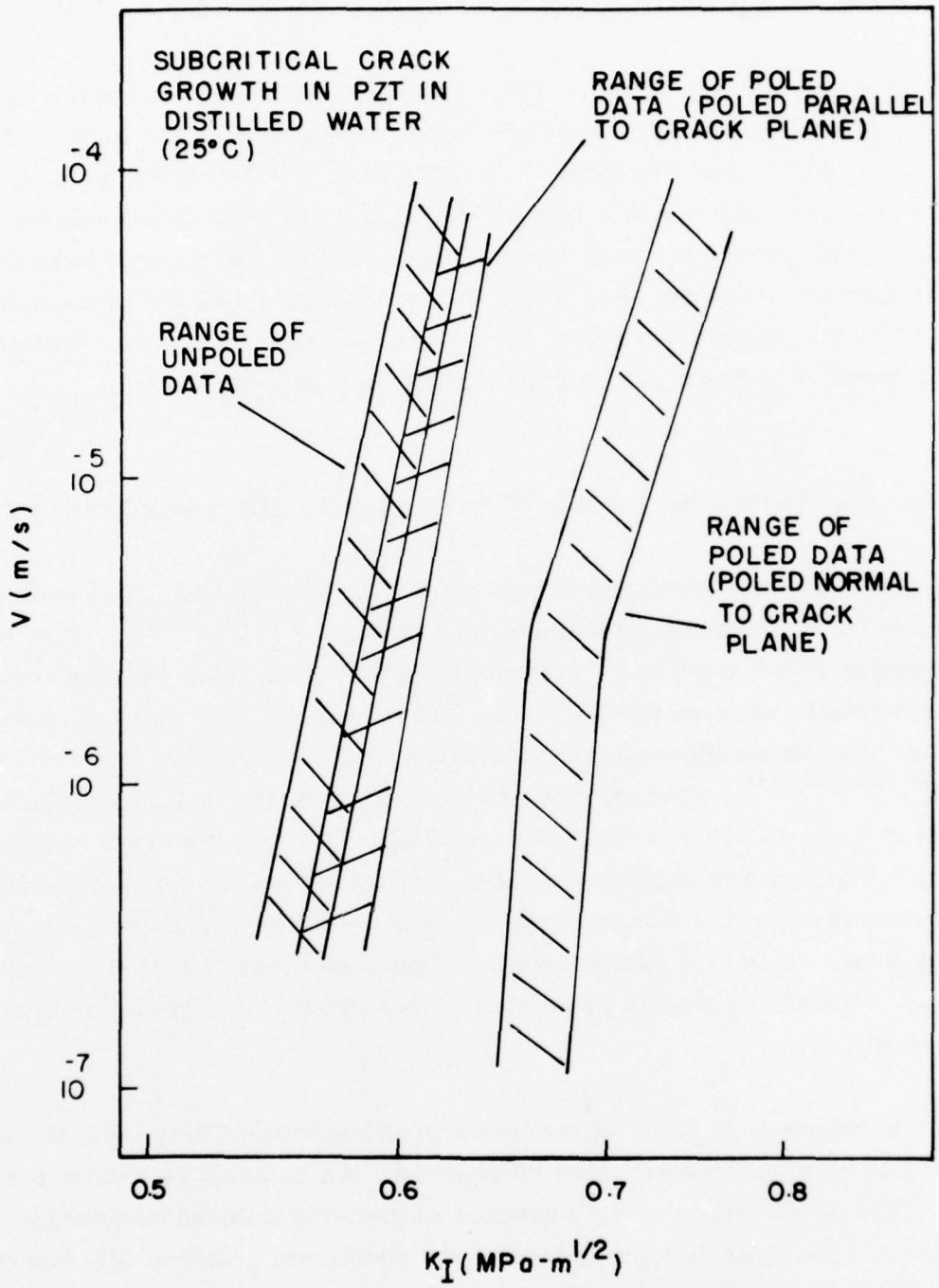

Figure 14. Plot showing the effect of poling on crack propagation in PZT in distilled water at 25°C. Note that poling parallel to the crack has little effect on crack propagation while poling perpendicular to the crack measurably retards crack propagation.

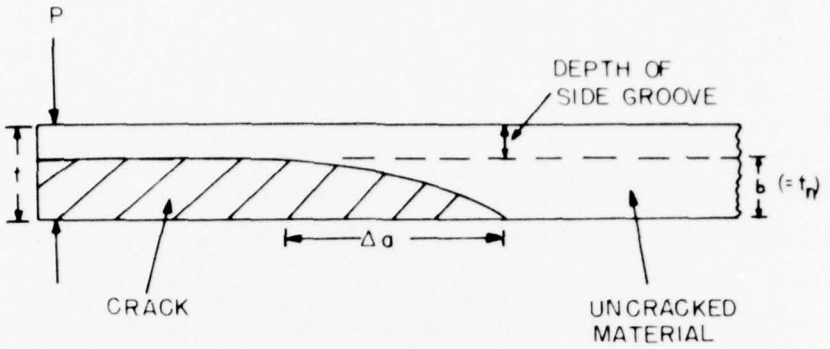

(a)

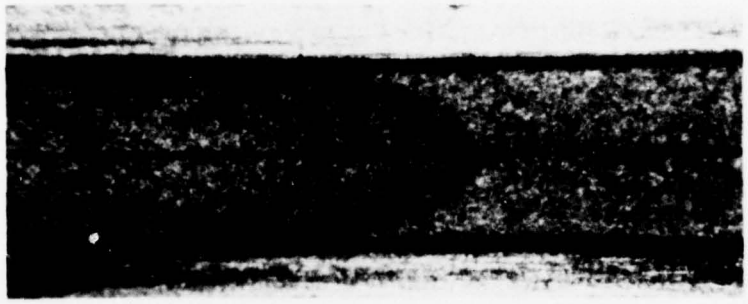

(b)

(c)

Figure 15. The crack profile in PZT double torsion specimens: (a) schematic, (b) normal crack profile, and (c) crack front intersecting the bottom surface at angle greater than 90 degrees.

The fracture paths of unpoled and poled specimens were notably different. Figure 16 shows the top views of two poled and one unpoled broken DT specimens. The fracture path in unpoled material was invariably straight, even when the samples were epoxied composites. In the poled samples, the fracture paths were generally wavy, as shown, regardless of poling direction. In all cases the cracks remained perpendicular to the specimen surface. We attribute the waviness to long range inhomogenieties in the microstructure or residual stress pattern resulting from corresponding inhomogenieties in the electrodes applied for poling.

A scanning electron micrograph of the fracture surface of an unpoled PZT specimen is shown in Figure 17a. With the exception of regions where the crack has intersected pores and pore clusters, crack propagation has occurred predominantly by transgranular fracture. Micrographs taken in regions of both slow and fast fracture revealed no difference in fracture appearance. The fracture surface of a specimen poled perpendicular to the crack is shown in Figure 17b. Fracture is again transgranular and, in general, the surface is quite similar to that of the unpoled specimen. The only notable difference is the appearance of some parallel arrays of markings visible on the poled surface. Presumably, the markings are due to the intersection of the crack with domain boundary patterns introduced by poling. Similar features were observed on the fracture surfaces of samples poled both parallel to (see Figure 15c) and perpendicular to the crack plane. No obvious differences were noted on the fracture surfaces that could account for the shift in the V-K_I curves to higher K_I when poling was perpendicular to the crack.

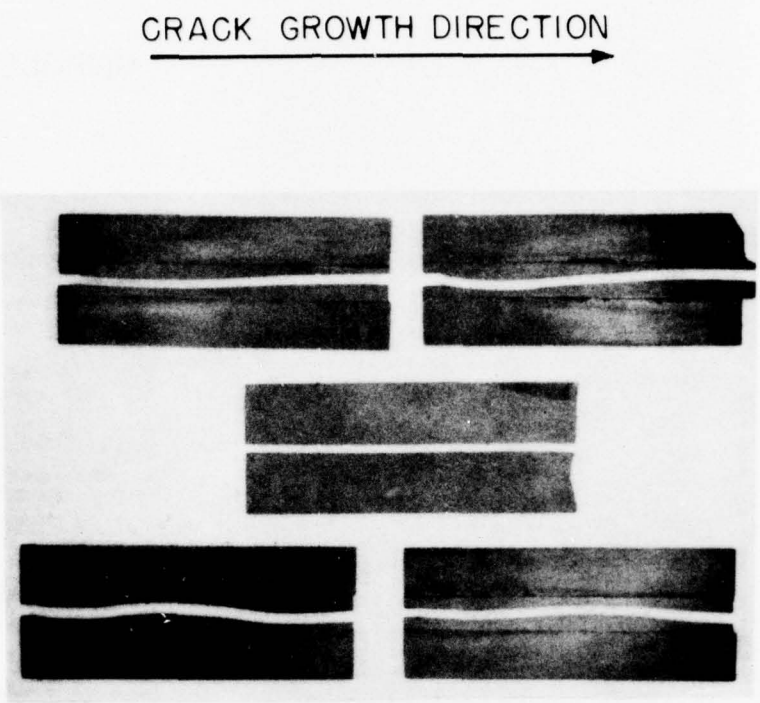

Figure 16. Photographs of broken PZT double torsion specimens showing straight crack path in unpoled material and wavy paths in poled material.

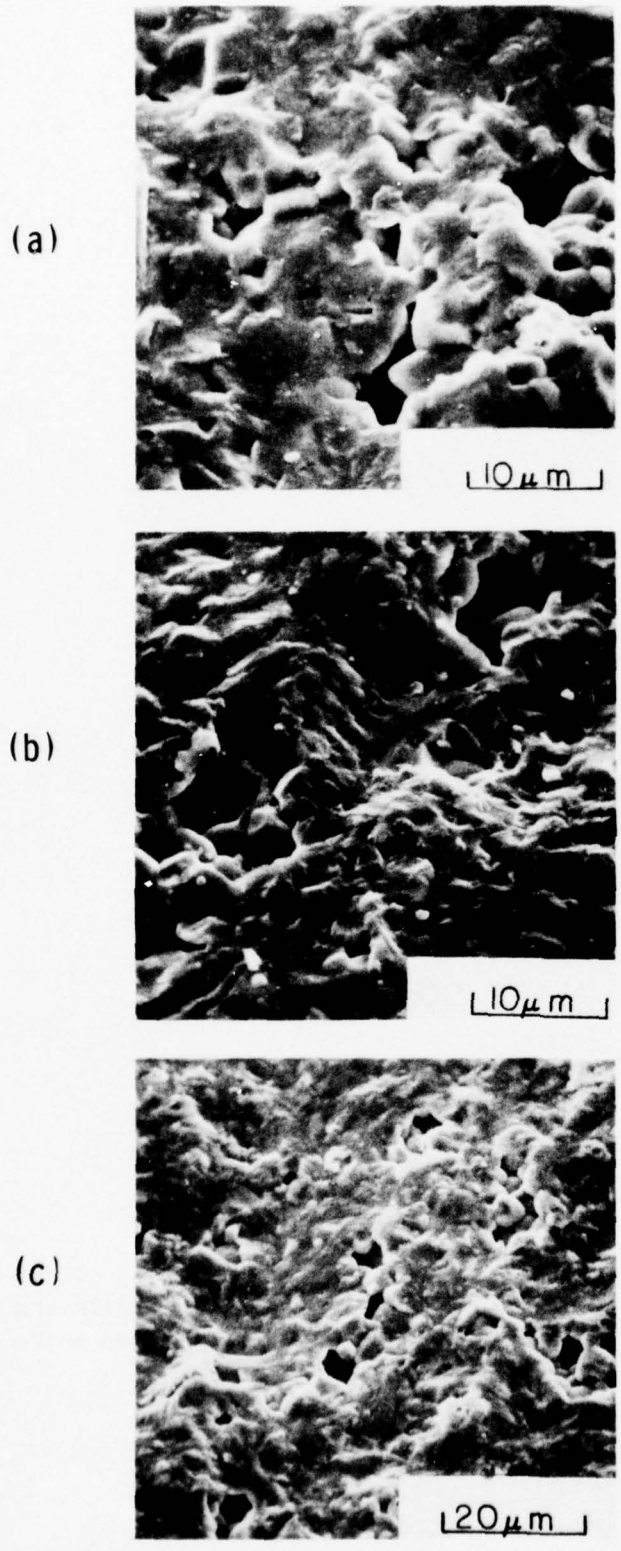

Figure 17. Scanning electron micrographs of the fracture surfaces of (a) unpoled PZT, (b) PZT poled perpendicular to crack and (c) PZT poled parallel to crack. Fracture is predominantly transgranular in all cases.

IV. DISCUSSION OF RESULTS

A. SPECIMEN DESIGN

It is significant to note that problems due to intermittent crack propagation during a DT relaxation test such as that shown schematically in Figure 4 can be essentially eliminated by using a specimen with a wide side groove. By widening the groove, the stress concentrations at the corners are removed to a distance from the propagating crack where they do not interact with the stress field of the crack. The crack geometry is then dominated by the outer fiber tensile stresses in the specimen and the crack, even though it may wander from the specimen center, is turned back towards the center and remains perpendicular to the specimen surface throughout a test. We suggest that adapting this aspect of the DT specimen geometry will increase the "yield" of valid DT tests and should be seriously considered by others using this type of test. The experimental results shown in Figure 5 and the analytical results of Trantina (16) further show that the starter crack should be at least as long as the specimen half width, W/2; otherwise, erroneously high values of K_I will be measured. If possible, specimens should be used that are longer than the ones employed in this study (i.e., 3W) to facilitate performing multiple relaxations. Multiple relaxations must give repeatable data if confidence in the results is to be expected.

B. ENVIRONMENTAL EFFECTS ON CRACK PROPAGATION IN UNPOLED PZT

The data shown in this report and by others[8, 9, 25] on the effects of environment on crack propagation in PZT conclusively show that PZT is susceptible to environmentally enhanced slow crack growth. Water appears to be the active medium. As shown in Figure 6, the V-K_I curves of PZT exhibit

three stages characteristic of other ceramics[7]. When the data are fitted to $V = AK_I^n$, n in Stage I is about 55 and in Stage III is about 130. The n values are slightly higher than those determined by Freiman, et. al.[8] for a PZT 5800 and are essentially identical to those found by Caldwell and Bradt[9] on another commercial PZT tested in air. This is an interesting point since the fracture mode was intergranular in Caldwell and Bradt's material, and was transgranular in ours and in that of Freiman et. al. From the $V-K_I$ data shown in Figures 6, 8, and 13, we further note that the operating lifetime of a component can be significantly extended if the service environment is a medium that is inert with respect to water. Stage I crack growth was essentially eliminated when tests were run in mineral oil and Freon.

Recent work has shown that the lifetimes of structural ceramic components can generally be predicted from $V-K_I$ data using proof testing techniques[7, 12]. In the case of transducer ceramics, however, a note of caution is in order. Transducers generally operate under cyclic loading conditions and data such as that shown in this report were obtained under "static" conditions. Evans and Fuller[26] have shown that $V-K_I$ curves under cyclic loading can be predicted from static $V-K_I$ data providing the characteristics of slow crack growth are not altered by the loading. It is not clear if this is the case in a transducer component. In an operating transducer, other effects such as that of a high applied field must also be considered. Preliminary studies[27] have shown, in fact, that $V-K_I$ data obtained with ac fields applied to a crack propagating in PZT are not the same as that predicted from the static $V-K_I$ curves using the analysis of Evans and Fuller[26].

C. CRACK PROPAGATION IN POLED PZT

Poling has been found to cause a measurable increase in the stress to propagate a crack only if the poling direction is perpendicular to the crack

plane. Only slight shifts in the V-K_I curves were noted when the poling direction was parallel to the crack plane. This behavior can be qualitatively accounted for by residual stresses introduced during poling. Since the PZT used in this study is predominantly tetragonal below the Curie temperature, polarization results from the switching of 90 - degree and 180 - degree domains[1]. Only 90 - degree domains, however, contribute to the strain accompanying polarization. When polycrystalline PZT is poled, 90 - degree domain rotation tends to deform each grain in the polarization direction. The deformation is, in turn, restricted by the surrounding grains and intergranular residual stresses result. One contribution to aging* in piezoelectric ceramics is, in fact, back switching of the 90 - degree domains due to residual poling stresses[1]. The residual stresses (and remanent strains) are highest in the poling direction. The residual stresses are compressive and will hinder crack propagation when the poling direction is perpendicular to the crack. A compressive stress parallel to the crack is not expected to interact strongly with the stress field at the crack tip, providing a maximum principal stress fracture criterion is controlling. Thus, cracks propagating in samples poled parallel to the crack plane show V-K_I behavior similar to unpoled samples.

The magnitude of the residual stress introduced by poling can be estimated from the shift, ΔK_I, in the V-K_I curves by considering how the residual stress alters the stress field of the crack. The maximum tensile stress in front of a Mode I crack is

$$\sigma_{yy} = \frac{K_I}{\sqrt{2\pi r}}$$

* Aging is the time dependent degradation of the dielectric properties of a ferroelectric material following poling, thermal treatments, or stress applications.

where r is the distance from the crack tip[28]. The stress in the presence of a residual stress, σ_r, is

$$\sigma_{yy}' = \frac{K'_I}{\sqrt{2\pi r}} - \sigma_r .$$

Fracture occurs in both cases when $\sigma_{yy} = \sigma_{yy}' = \sigma_F$ where σ_F is the fracture stress. Thus

$$\sigma_r = \frac{K'_I - K_I}{\sqrt{2\pi r}} = \frac{\Delta K}{\sqrt{2\pi r}} .$$

At distances from the crack tip corresponding to realistic flaw sizes in PZT, e.g., 10 to 50 μm, the residual stress is about 6 to 13 MNm^{-2}, which is reasonable.

An alternate explanation of the effects of poling on crack propagation is based on the interaction of a crack with the different microstructures of poled and unpoled material. Gerson[29] has shown, for instance, that the density of both 90 - degree and 180 - degree domain boundaries in PZT decrease drastically after poling. The resulting "coarser" microstructure could lead to higher fracture energies. The removal of domain boundaries upon poling does not, however, account for the large anisotropy observed in fracture energy with respect to poling direction. The fact that poled and unpoled material exhibited V-K_I curves with similar shapes* when tested in a number of environments also indicates that the presence (or absence) of domain boundaries plays a minor role in the fracture process in PZT[30].

* But shifted to higher values of K_I when poling was perpendicular to the crack.

Fracture Mechanism

As shown in Figure 11, the apparent activation energy for slow crack propagation in unpoled PZT in water is a linear function of K_I and extrapolates to a stress-free activation energy of about 100 kcal/mol. If the bond energy is defined as the oxide dissocation energy divided by the coordination in the Perovskite structure[31] the following table indicates that the measured value is about 30 percent higher than either the Zr-O or Ti-O bond energies which, in PZT, are presumably rate controlling.

Cation	Coordination Number in PZT	Oxide Dissociation Energy (Kcal/mol)	Bond Energy (Kcal/mol)
Pb	12	145	12
Ti	6	435	72
Zr	6	485	81

Other rate controlling mechanisms might be associated with the stress-enhanced diffusion of some species near the crack tip. However, the observed stress fee activation energy is too high for reasonable candidates. Furthermore, if stress enhanced diffusion were important, one would expect the samples poled parallel to the crack to exhibit $V\text{-}K_I$ behavior different from that of unpoled material. That is, since V can be related to the pressure tensor gradient driving the "embrittling species" by [32]

$$V \alpha \frac{d\sigma_{ii}}{dx} \text{ and } \sigma_{ii} = \sigma_x + \sigma_y + \sigma_z \qquad (4)$$

if σ_x is decreased as a result of the poling induced residual compressive stress, then the velocity should decrease. Since this is not the case, a normal stress criterion for the cohesive bond is much more realistic in the present case.

Clearly more activation energy measurements will be needed in inert environments and in poled material before fracture in PZT is better understood. A major experimental probelm in studying thermally activated crack propagation in PZT, however, is that while the test temperatures were low with respect to the melting point, they were high with respect to the Curie temperature and close to the morphotropic boundary. Any stress and/or temperature induced structural changes complicate the application of a simple thermal activation analysis.

Two other aspects of fracture in PZT deserve mention. These are the possible existence of a deformed zone at the crack tip resulting from the stress induced migration of 90 - degree domain boundaries[1, 33] and the resulting electrostrictive charge buildup. Both will tend to hinder crack propagation, but, since they are stress dependent, should not be reflected in the stress free activation energy. If the dependence of these effects on stress is not linear, however, a linear extrapolation to determine the activation energy is not justified.

V. ACKNOWLEDGEMENTS

The authors are indebted to Drs. R. J. Stokes, R. G. Johnson, and W. W. Gerberich for helpful and critical discussion and to S. J. Tibbetts for experimental assistance during the course of this study. The continued interest of Dr. A. N. Diness, Office of Naval Research, is gratefully acknowledged.

VI. REFERENCES

1. B. Jaffe, W. Cook Jr. and H. Jaffe, Piezoelectric Ceramics, Academic Press, New York, (1971).

2. B. K. Molnar and R. W. Rice, Bull. Am. Ceram. Soc., 52, 505 (1973).

3. R. C. Pohanka, et. a., Proc. Workshop on Sonar Transducer Mater., P. L. Smith and R. C. Pohanka, ed., Naval Res. Lab (1976), p. 205.

4. R. W. Rice in Fracture Mechanics of Ceramics, Vol. 1, R. C. Bradt, D. P. H. Hasselman and F. F. Lange, ed., Plenum Publishing Co., New York (1974) p. 323.

5. R. G. Johnson, Honeywell Corporate Material Sciences Center, private communication (1977).

6. R. C. Pohanka, S. W. Freiman and B. E. Walker, Bull. Am. Ceram. Soc., 56, 291 (1977) (abstract only).

7. A. G. Evans and T. G. Langdon, Prog. Mat. Sci., 21, 171 (1976).

8. S. W. Freiman, K. R. McKinney and H. L. Smith, in Fracture Mechanics of Ceramics, Vol. 2, R. C. Bradt, D. P. H. Hasselman and F. F. Lange, ed., Plenum Publishing Co., New York, (1974) p. 659.

9. R. F. Caldwell and R. C. Bradt, J. Am. Ceram. Soc., 60, 168 (1977).

10. A. G. Evans, J. Mater. Sci., 7, 1137 (1972).

11. D. P. Williams and A. G. Evans, J. Testing and Eval., 1, 264 (1973).

12. S. M. Wiederhorn, p. 613 in reference 7.

13. S. M. Wiederhorn, National Bureau of Standards, Private communication (1975).

14. P. H. Hodkinson and J. S. Nadeau, J. Mater. Sci., 10, 846 (1975).

15. B. J. Pletka, National Bureau of Standards, private communication (1977).

16. G. G. Trantina, to be published in J. Am. Ceram. Soc. (1977).

17. S. M. Wiederhorn, J. Am. Ceram. Soc., 52, 99 (1969).

18. D. K. Shetty and A. V. Virkar, Bull, Am. Ceram. Soc., 56, 301 (1977) (abstract only).

19. S. W. Freiman, D. R. Mulville and P. W. Mast, J. Mater. Sci., 8, 1527 (1973).

20. R. W. Adams and P. W. McMillan, J. Mater. Sci., 12, 643 (1977).

21. A. G. Evans and E. A. Charles, J. Am. Ceram. Soc., 59, 371 (1976).

22. W. W. Gerberich and M. Stout, J. Am. Ceram. Soc., 59, 222 (1976).

23. J. S. Nadeau, J. Am. Ceram. Soc., 57, 303 (1974).

24. A. K. Virkar and R. S. Gordan, J. Am. Ceram. Soc. 58, 536 (1975).

25. R. Sedlack and V. Salman, Final Tech. Report Con. No. NOO24-70-C-1224, Naval Ship Systems Command (1971), references by Freiman et.al., *in reference* 7.

26. A. G. Evans and E. R. Fuller, Met. Trans., 5, 27 (1974).

27. R. G. Johnson, S. J. Tibbetts, J. G. Bruce and B. G. Koepke, Bull. Am. Ceram. Soc., 56, 302 (1977) (abstract only).

28. G. R. Irwin and P. C. Paris in Fracture an Advanced Treatise, Vol. III, H. Liebowitz ed., Academic Press, New York (1971) p. 1.

29. R. Gerson, J. Appl. Phys. 31, 188 (1960).

30. This point came out during a discussion with R. Pohanka, Naval Res. Lab.

31. K. H. Sun, J. Am. Ceram. Soc., 30, 277 (1947).

32. W. W. Gerberich, Y. T. Chen and C. St. John, Met. Trans., 6A, 1485 (1975).

33. E. C. Subbarao, M. C. McQuarrie and W. R. Buessem, J. Appl. Phys., 28, 1194 (1957).

BASIC DISTRIBUTION LIST October 1976

Technical and Summary Reports

Organization	No. of Copies
Defense Documentation Center Cameron Station Alexandria, Virginia 22314	(12)
Office of Naval Research Department of the Navy	
Attn: Code 471	(1)
Code 102	(1)
Code 470	(1)
Commanding Officer Office of Naval Research Branch Office 495 Summer Street Boston, Massachusetts 02210	(1)
Commanding Officer Office of Naval Research Branch Office 536 South Clark Street Chicago, Illinois 60605	(1)
Office of Naval Research San Francisco Area Office 760 Market Street, Room 447 San Francisco, California 94102	
Attn: Dr. P. A. Miller	(1)
Naval Research Laboratory Washington, D.C. 20390	
Attn: Code 6000	(1)
Code 6100	(1)
Code 6300	(1)
Code 6400	(1)
Code 2627	(1)
Naval Air Development Center Code 302 Warminster, Pennsylvania 18974	
Attn: Mr. F. S. Williams	(1)
Naval Air Propulsion Test Center Trenton, New Jersey 08628	
Attn: Library	(1)
Naval Construction Batallion Civil Engineering Laboratory Port Hueneme, California 93043	
Attn: Materials Division	(1)
Naval Electronics Laboratory Center San Diego, California 92152	
Attn: Electron Materials Sciences Division	(1)
Naval Missile Center Materials Consultant Code 3312-1 Point Mugu, California 93041	(1)
Commanding Officer Naval Surface Weapons Center White Oak Laboratory Silver Spring, Maryland 20910	
Attn: Library	(1)
David W. Taylor Naval Ship R&D Center Materials Department Annapolis, Maryland 21402	(1)
Naval Undersea Center San Diego, California 92132	
Attn: Library	(1)
Naval Underwater System Center Newport, Rhode Island 02840	
Attn: Library	(1)
Naval Weapons Center China Lake, California 93555	
Attn: Library	(1)
Naval Postgraduate School Monterey, California 93940	
Attn: Mechanical Engineering Dept.	(1)
Naval Air Systems Command Washington, D.C. 20360	
Attn: Code 52031	(1)
Code 52032	(1)
Code 320	(1)

Organization	No. of Copies
Naval Sea System Command Washington, D.C. 20362 Attn: Code 035	(1)
Naval Facilities Engineering Command Alexandria, Virginia 22331 Attn: Code 03	(1)
Scientific Advisor Commandant of the Marine Corps Washington, D.C. 20380 Attn: Code AX	(1)
Naval Ship Engineering Center Department of the Navy CTR BG #2 3700 East-West Highway Prince Georges Plaza Hyattsville, Maryland 20782 Attn: Engineering Materials and Services Office, Code 6101	(1)
Army Research Office Box CM, Duke Station Durham, North Carolina 27706 Attn: Metallurgy & Ceramics Div.	(1)
Army Materials and Mechanics Research Center Watertown, Massachusetts 02172 Attn: Res. Programs Office (AMXMR-P)	(1)
Air Force Office of Scientific Research Bldg. 410 Bolling Air Force Base Washington, D.C. 20332 Attn: Chemical Science Directorate Electronics and Solid State Sciences Directorate	(1) (1)
Air Force Materials Lab (LA) Wright-Patterson AFB Dayton, Ohio 45433	(1)
NASA Headquarters Washington, D.C. 20546 Attn: Code RRM	(1)
NASA Lewis Research Center 21000 Brookpark Road Cleveland, Ohio 44135 Attn: Library	(1)
National Bureau of Standards Washington, D.C. 20234 Attn: Metallurgy Division Inorganic Materials Division	(1) (1)
Defense Metals and Ceramics Information Center Battelle Memorial Institute 505 King Avenue Columbus, Ohio 43201	(1)
Director Ordnance Research Laboratory P.O. Box 30 State College, Pennsylvania 16801	(1)
Director Applied Physics Laboratory University of Washington 1013 Northeast Fortieth Street Seattle, Washington 98105	(1)
Metals and Ceramics Division Oak Ridge National Laboratory P.O. Box X Oak Ridge, Tennessee 37380	(1)
Los Alamos Scientific Laboratory P.O. Box 1663 Los Alamos, New Mexico 87544 Attn: Report Librarian	(1)
Argonne National Laboratory Metallurgy Division P.O. Box 229 Lemont, Illinois 60439	(1)

BASIC DISTRIBUTION LIST (Cont'd)

Organization	No. of Copies
Brookhaven National Laboratory Technical Information Division Upton, Long Island New York 11973 Attn: Research Library	(1)
Library Building 50 Room 134 Lawrence Radiation Laboratory Berkeley, California	(1)

TP
March 1977

SUPPLEMENTARY DISTRIBUTION LIST

Technical and Summary Reports

Advanced Research Projects Agency
Materials Science Director
1400 Wilson Boulevard
Arlington, VA 22209

Professor Michael Bell
Yeshiva University
Belfer Graduate School of Science
New York, NY 10033

Dr. Don Berlincourt
Channel Products
16722 Park Circle Dr. W.
Chagrin Falls, OH 44022

Dr. J. V. Biggers
Pennsylvania State University
Materials Research Laboratory
University Park, PA 16802

Mr. George Boyer
Sensor Systems Program
Office of Naval Research
Code 222
Arlington, VA 22217

Professor R. Bradt
Ceramics Section
Materials Sciences Department
The Pennsylvania State University
University Park,, PA 16802

Dr. Dean Buckner
Piezo Products Division
Gulton Industries
P.O. Box 4300
Fullerton, CA 92634

Dr. Robert Callahan
Channel Industries
839 Ward Drive
Box 3680
Santa Barbara, CA 93105

Professor L. E. Cross
The Pennsylvania State University
Materials Research Laboratory
University Park, PA 16802

Mr. N. Coda
Vice President for Engineering
Erie Technological Products
West College Avenue
State College, PA 1680

Dr. A. G. Evans
Rockwell International
P.O. Box 1085
1049 Camino Dos Rios
Thousand Oaks, CA 91360

Dr. Richard Fulrath
University of California
266 Hearst Mining Building
Berkeley, CA 94720

Dr. Gene Haertling
Motorola Corporation
3434 Vassar, NE
Albuquergue, NM 87107

Mr. W. B. Harrison
Honeywell Ceramics Center
1885 Douglas Drive
Golden Valley, MN 55422

Dr. D. P. H. Hasselman
Virginia Polytechnic Institute
Department of Materials Sciences
Blacksburg, VA

Dr. L. L. Hench
Department of Metallurgy
University of Florida
Gainesville, FL 32603

Dr. A. H. Heuer
Professor of Ceramics
Case Western Reserve University
University Circle
Cleveland, OH 44106

Dr. F. Robert Hill
Marine Resources
755 Highway 17 & 92
Fern Park, FL 32730

SUPPLEMENTARY DISTRIBUTION LIST (CONT"D)

Dr. Bernard Jaffe
232 Forbes Road
Bedford, OH 44146

Dr. Paul Jorgensen
Stanford Research Institute
333 Ravenswood Avenue
Menlo Park, CA 94025

Dr. R. N. Katz
Army Materials and Mechanics
Research Center
Watertown, MA 02172

Dr. H. Kirchner
Ceramic Finishing Company
P. O. Box 498
State College, PA 16801

Dr. B. G. Koepke
Honeywell, Inc.
Corporate Research Center
10701 Lyndale Avenue South
Bloomington, MN 55420

Mr. Frank Koubek
Naval Surface Weapons Center
White Oak Laboratory
Silver Spring, MD 20910

Dr. J. Lankford
Southwest Research Institute
8500 Culebra Road
San Antonio, TX 78284

Dr. R. Lapetina
Edo Western Corporation
2645 South 300 West
Salt Lake City, UT 84115

Mr. C. LeBlanc
Naval Underwater Systems Center
TD 121
Newport, RI 02840

Dr. R. E. Loehman
University of Florida
Ceramics Division
Gainesville, FL 32601

Professor P. B. Macedo
The Catholic University of America
Washington, DC 20017

Dr. N. Perrone
Code 474
Office of Naval Research
800 N. Quincy Street
Arlington, VA 22217

Dr. R. Pohanka
Naval Research Laboratory
Code 6130
Washington, DC 20375

Dr. R. Rice
Naval Research Laboratory
Code 6360
Washington, DC 20375

Dr. Frank Recny
General Electric Company
Court Street
Plant Building C
Box 1122
Syracuse, NY 13201

Dr. J. H. Rosolowski
General Electric Company
Research and Development Center
P.O. Box 8
Schenectady, NY 02301

Dr. D. A. Shockey
Stanford Research Institute
Poulter Laboratory
Menlo Park, CA 94025

Dr. J. H. Simmons
Catholic University of America
Washington, DC 20064

Dr. P. L. Smith
Naval Research Laboratory
Code 6361
Washington, DC 20375

SUPPLEMENTARY DISTRIBUTION LIST (CONT'D)

Dr. R.W. Timme
Naval Research Laboratory
Code 8275
Underwater Sound Reference Division
P.O. Box 8337
Orlando, FL 32806

Dr. Charles C. Walker
Naval Sea Systems Command
National Center #3
2531 Jefferson Davis Highway
Arlington, VA 20390

Dr. Paul D. Wilcox
Sandia Laboratories
Division 2521
Albuquerque, NM 87115

The State University of New York
at Alfred
Material Sciences Division
Alfred, NY 14802

Dr. N.S. Corney
Ministry of Defense
(Procurement Executive)
The Adelphi
John Adam Street
London WC2N 6BB
UNITED KINGDOM

Dr. Murray Gillen
Australian Embassy
Washington, DC 33801

Dr. D.J. Godfrey
Admiralty Materials Laboratory
Ministry of Defense
(Procurement Executive)
Holton Heath
Poole, Dorset
BH16 6JU
UNITED KINGDOM

Linda Husted
Librarian
Materials Sciences Corporation
Merion Towle Building
Blue Bell, PA 19422

Globe-Union, Inc.
5757 North Green Bay Avenue
Milwaukee, WI 53201
ATTN: G. Goodman

Prof. P.J. Gielisse
Dept. of Chemical Engineering
University of Rhode Island
Kingston, RI 02881

Dr. M. Noone
General Electric Company
Space Sciences Laboratory
Room M9539, P.O. Box 8555
Philadelphia, PA 19101

Dr. R.N. Katz
Army Mechanics and Materials
Research Center
Watertown, MA 02172

Mr. W.B. Crandall
Alfred University
Alfred, NY 14802

Dr. J.T.A. Roberts
Electric Power Research Institute
3412 Hillview Ave.
P.O. Box 10412
Palo Alto, CA 94303

Dr. W.R. Manning
Champion Spark Plug Company
20000 Conner Ave.
Detroit, MI 48234

Dr. G.K. Bansal
Battelle
505 King Avenue
Columbus, OH 43201

Dr. B.A. Wilcox
Ceramics Program, Room 336
Metallurgy and Materials Research
National Science Foundation
Washington, D.C. 20550

Dr. H.E. Bennett
Naval Surface Weapons Center
Research Department Code 601
China Lake, CA 93555

SUPPLEMENTARY DISTRIBUTION LIST (CONT'D)

Dr. R.J. Charles
General Electric Company
Research and Development Center
Schenectady, NY 12301

Dr. A.R.C. Westwood
Martin-Marietta Laboratories
1450 South Rolling Road
Baltimore, MD 21227

Professor R.H. Doremus
Rensselaer Polytechnic Institute
Troy, NY 12181

Dr. D.E. Niesz
Battelle Memorial Institute
505 King Avenue
Columbus, OH 43201

Dr. S.M. Wiederhorn
Inorganic Materials Division
National Bureau of Standards
Washington, D.C. 20234

Dr. C.O. Hulse
United Aircraft Research Labs
United Aircraft Corporation
East Hartford, CT 06108

Prof. M.H. Manghnani
University of Hawaii
Hawaii Institute of Geophysics
2525 Correa Road
Honolulu, HI 96822

Dr. Marvin Hass
Naval Research Laboratory
Code 6408
Washington, D.C. 20375

Dr. S.M. Wiederhorn
Physical Properties Section
Bldg. 223, Rm. A355
National Bureau of Standards
Washington, D.C. 20234

Dr. P.F. Becher
Code 6362
U.S. Naval Research Laboratory
Washington, D.C. 20375